Desalination and Water Treatment
www.deswater.com
doi: 10.5004/dwt.2020.24937

178 (2020) 283–295
February

Adsorption performance of expanded graphite and its binary composite microbeads toward oil and dyes

Yayu Tian, Ning Zhang, Yue Liu, Wenjuan Chen, Renjie Lv, Hongzhu Ma*

Key Laboratory of Applied Surface and Colloid Chemistry, Ministry of Education, School of Chemistry and Chemical Engineering, Shaanxi Normal University, Xi'An, Shaanxi, 710119, China, Tel. +86 29 81530726; Fax: +86 29 81530727;
emails: hzmachem@snnu.edu.cn (H. Ma), 417806756@qq.com (Y. Tian), 934073433@qq.com (N. Zhang), 478420167@qq.com (Y. Liu), 1745147310@qq.com (W. Chen), 754600255@qq.com (R. Lv), hzmachem@snnu.edu.cn (H. Ma)

Received 13 March 2019; Accepted 21 September 2019

ABSTRACT

In this study, expanded graphite (EG) by an environmentally friendly and mild oxidation intercalation and binary composite microbeads adsorbent (EG-*x*Gel) was prepared to purify dye and oily wastewater. The synthesized EG and EG-*x*Gel were characterized. A characteristic homogeneous dilation and vermicular structure with interconnected pores for EG and relatively uniform spherical with well dispersion for EG-64Gel were detected. Within 30 min, the adsorption amount of EG to engine and edible oil reached 23.89 and 26.03 g g^{-1}, respectively. In the oily wastewater system, the corresponding amount increased slightly from 22.25 to 23.97 g g^{-1}, and 26.38 to 30.92 g g^{-1} respectively, with the introduction of 15 g L^{-1} NaCl, which might be due to the higher ionic strength reduced the solubility of the adsorbate in the solution. The highest removal of 68.2% and 87.2% was observed for 50 mg L^{-1} methylene blue (MB) at the original pH for 2 h and congo red (CR) at pH 3 for 40 min, respectively, with 0.1 g EG-64Gel microbeads by air dried applied at room temperature. The pseudo-second-order kinetics described MB and CR adsorption process better. Moreover, EG-64Gel exhibited excellent separation performance under acidic condition with CR dye almost removed completely in the binary MB/CR system. All these results indicated that EG and EG-*x*Gel are expected to be promising candidates for the frequent oil-spill accidents and dye wastewater pollution.

Keywords: Gelatin; Expanded graphite; Adsorption; Oily substrates; Dyes

1. Introduction

Marine oil pollution is one of the environmental concerns that are currently becoming major issues in the petroleum industry, which may arise from oil run-offs from onshore facilities or oil tanker spills during transportation [1–3], and has become more severe with increasing petroleum activities [4,5]. Nowadays, the pollution of dye wastewater to surface water and groundwater also has become a global environmental problem, which poses a great threat to human and aquatic life.

Frequent oil-spill accidents and dye wastewater pollution not only cause severe and long-term damages to marine ecosystems but also lead to a great loss of valuable resources [6,7]. To eliminate the environmental pollution of oil spills quickly, an efficient and environmentally friendly oil-recovery approach is highly demanded. As one of the most effective process with high efficiency and ease to apply in industries, adsorption has attracted much attention in various technologies [8–14].

Carbon-based material is a commonly used adsorbent for oil pollution and effluents treatment. Expanded graphite

* Corresponding author.

(EG) is an inorganic porous carbon-based adsorbent with a low density, and usually prepared from well-crystallized natural flake graphite [15]. Because of its high lipophilic and hydrophobic properties, EG can selectively remove the oil slick in sea and lake with clumping up and floating on the liquid surface for easy collection and disposal [16]. Li et al. [17] applied EG to the removal of various dyes such as disperse blue 2BLN, acid black 210 and direct scarlet 4BS from aqueous solutions, and found that the removal process was relatively time consuming. Gelatin (Gel) is a straight-chain polymer produced by controlling the hydrolysis of collagen with good biodegradability and hydrophilicity [18].

In this study, expanded graphite (EG) and its binary composite microbeads with gelatin (EG-*x*Gel) were prepared. The parameters such as ultrasonic time, drying temperature and time were optimized. The surface morphologies, composition and thermal stability of samples were characterized by scanning electron microscopy (SEM), Fourier transform infrared spectra (FT-IR) and thermogravimetric analysis (TGA). The adsorption properties of EG toward five different oily substrates were evaluated, and the effects of salt content, temperature and contact time on its adsorption properties were studied. The tunable adsorption property of EG-*x*Gel toward congo red (CR) and methylene blue (MB) was investigated by changing the mass ratio of EG to gelatin. The effects of way of drying, contact time and initial pH of solution on the adsorption of CR and MB onto EG-64Gel were investigated. Its selective adsorption property in MB/CR binary system was evaluated under the co-presence of inorganic salt NaCl and various pHs. The swelling property and the consecutive adsorption recycle of EG-64Gel were also investigated. In addition, the kinetics of adsorption process was discussed.

2. Materials and methods

2.1. Materials

Natural flake graphite (NG, 99%, grain size 50 mesh) was purchased from Kim To Qingdao Graphite Co. Ltd. (China). Ammonium persulfate ($(NH_4)_2S_2O_8$), concentrated sulfuric acid (H_2SO_4), benzene (C_6H_6), *n*-heptane (n-C_7H_{14}), *p*-xylene (C_8H_{10}), anhydrous ethanol (C_2H_5OH), acetone (CH_3COCH_3), methylene blue ($C_{16}H_{18}N_3ClS$), congo red ($C_{32}H_{22}N_6Na_2O_6S_2$) in A.R. were supplied by Sinopharm Chemical Reagent Co. Ltd., (Shanghai, China). Gelatin was supplied by Xi'an Guo'an Biotechnology Co. Ltd., (Xi'an, China). Sunflower oil was supplied by Yihai Kerry Food Co. Ltd., (Hong Kong, China). Triply distilled water was used in all experiments.

The synthetic wastewater was prepared in laboratory by dissolving proper amount of commercial dyes in distilled water.

2.2. Preparation of expanded graphite and EG-xGel microbeads

2.2.1. Preparation of expanded graphite

Expanded graphite (EG) derived from natural flake graphite was prepared according to the literature [19]. Briefly, $(NH_4)_2S_2O_8$ (5.00 g) was mixed with H_2SO_4 (3 mL) at room temperature and stirred continuously for 15 min, and treated in an ultrasonic cleaning bath at 100 W (KQ-5200DE, Kunshan Ultrasonic instrument Co. Ltd., Jiangsu) for 5 min, then added to 1.00 g natural flake graphite (NG) and further treated by ultrasonic for 0–50 min at 80°C, then dried at 40°C–120°C for 15–60 min for further expansion. After that, the solid was washed to neutral and dried to obtain EG.

The expansion volume (V_E, mL g^{-1}) of EG was calculated as Eq. (1).

$$V_E = \frac{V}{m} \tag{1}$$

where V and m are the volume (mL) and mass (g) of EG, respectively.

2.2.2. Preparation of EG-xGel microbeads

Various amounts of EG were added into 10 mL acetone and dispersed by ultrasound at 100 W for 30 min to obtain EG dispersion [20]. The gelatin powder was dissolved in deionized water with stirring at 60°C, then introduced slowly into EG dispersion, and stirred overnight at 45°C. The obtained uniform solution was dropwise added into 200 mL cold sunflower oil with a 5 mL syringe under continuously stirring, and then kept in an ice water mixture for 2 h. The produced microbeads were separated and washed with distilled water and ethanol several times, and dried at room temperature. The obtained composite microbeads were denoted as EG-*x*Gel (*x* is the mass ratio of Gel to EG, *x* = 64, 48 and 24).

2.3. Characterization

Fourier transformed infrared spectroscopy (FT-IR, Tensor27, Bruker, Germany) analyses were performed in the range of 4,000–400 cm^{-1} with KBr pellets. The surface morphologies of the samples were observed by scanning electron microscope (TM3030, Hitachi Limited, Tokyo, Japan), after the deposition of a thin gold layer on the surface of the samples. The thermal stability of natural graphite, expanded graphite, gelatin and EG-64Gel was tested using TGA (Q600SDT, USA), with a temperature range of 25°C–800°C at a scanning rate of 10°C/min under nitrogen atmosphere. The Zeta potentials of the EG-64Gel composite microspheres at different pH values were determined with Zetasizer Nano ZS (Malvern Instruments Ltd., UK).

2.4. Evaluation of adsorption performance of expanded graphite and EG-xGel

2.4.1. Adsorption performance of expanded graphite toward various single oil substrates

Several oily substrates, such as engine oil, edible oil, benzene, *n*-heptane and *p*-xylene, were chosen as the simulated single spills oil system, to investigate the adsorption capacities of EG. A certain amount of EG was immersed into an above-mentioned single system. After 30 min, the adsorbed EG was separated and measured, the adsorption quantity q_t (g g^{-1}) was calculated according to Eq. (2).

$$q_t = \frac{m_2 - m_1}{m_1} \tag{2}$$

where m_1, m_2 are the mass of EG before and after adsorption, respectively.

2.4.2. Selective adsorption performance of expanded graphite in oily wastewater system

The mixture of edible oil or engine oil and water in volume ratio 1:4 was selected as the simulated oily wastewater. A certain amount of EG was added into the mixture system with constant stirring. At a certain interval, the volume of distilled water was measured after standing, the mass of EG before and after adsorption was recorded, and the adsorption quantity was calculated according to Eq. (2). The effects of temperature and NaCl at various concentrations (1, 5, 10 and 15 g L^{-1}) on its adsorption properties were evaluated.

2.4.3. Adsorption of expanded graphite and EG-xGel microbeads toward methylene blue and Congo red dyes

Congo red (CR) and methylene blue (MB) were chosen as the representative anionic and cationic dyes, due to their wide utilization. Typically, 0.10 g adsorbent was added into 10 mL of 50 mg L^{-1} MB or CR dye solution. 0.05 M HCl or 0.2 M NaOH was employed for pH adjustment. All the sorption experiments were carried out in duplicate. The concentration of the dye was determined using a UV-vis spectrophotometer (UVT6, Beijing Purkinje General Instrument Co. Ltd., China) at the maximum absorbance wavelength (662 nm for MB and 500 nm for CR, respectively).

The removal efficiency (R%) of the dyes was calculated according to Eq. (3):

$$R\% = -\frac{A_0 - A_t}{A_0} \times 100\% = \frac{C_0 - C_t}{C_0} \times 100\% \tag{3}$$

where A_0 and A_t are the respective dye absorbance in solution at initial time and at time t, C_0 and C_t are the respective dye concentration (mg L^{-1}) in solution at initial time and at time t.

2.4.4. Selective adsorption properties of EG-64Gel microbeads in MB/CR binary system

5 mL MB solution (50 mg L^{-1}, pH 7.15) and 5 mL CR solution (50 mg L^{-1}, pH 3.13) were carefully mixed to form a MB/CR binary dye system. Then 0.10 g EG-64Gel composite microbeads were added, and the effects of contact time, initial pH and presence of various concentrations of NaCl on the selective adsorption performance of EG-64Gel composite microbeads were investigated by detecting UV-vis spectroscopy of binary dyes solution in the range of 300–800 nm at room temperature, especially the absorbance at the maximum absorbance wavelength of dyes.

2.5. Desorption and recycle performance of EG-64Gel microbeads

0.10 g EG-64Gel microbeads were immersed into 10 mL dye solution (50 mg·L^{-1}). When the adsorption equilibrium reached, the adsorbed EG-64Gel microbeads were separated by centrifuge and then put into 50 mL of CH_3CH_2OH as desorption solution. The concentration of dye solution was analyzed and the desorption ratio (D%) was calculated as Eq. (4):

$$D\% = \frac{C_d V_d}{\left(C_0 - C_e\right) V_i} \times 100\% \tag{4}$$

where C_0 and C_e are concentrations (mg L^{-1}) of dye solution at initial time and equilibrium time, respectively. C_d is the concentration of dye in the desorption solution (mg L^{-1}). V_i and V_d are the volumes of the adsorption and desorption solution (mL), respectively. After desorption, the recovered adsorbent was separated by centrifuge, washed several times by distilled water and then immersed into the dye solution again for reuse.

2.6. Swelling behavior of EG-64Gel microbeads

An appropriate amount of the composite beads EG-64Gel was dried at room temperature and then put into 10 mL of deionized water until the swelling equilibrium was achieved. The swollen microbeads were separated and dried superficially with filter paper. The swelling ratio (S%) was calculated according to Eq. (5):

$$S\% = \frac{W_s - W_i}{W_i} \times 100\% \tag{5}$$

where W_i and W_s are the weights of composite microbeads at initial and time t.

2.7. Adsorption kinetics

The adsorption quantity of CR and MB at various contact time onto EG-64Gel at 298 K was analyzed by two kinetic models including pseudo-first-order and pseudo-second-order kinetics [21,22], as given in Eqs. (6) and (7):

$$\log\left(q_e - q_t\right) = \log q_e - \frac{k_1}{2.303} t \tag{6}$$

$$\frac{t}{q_t} = \frac{1}{k_2 q_e^2} + \frac{1}{q_e} t \tag{7}$$

where k_1 and k_2 are the pseudo-first-order and pseudo-second-order rate constants, respectively, q_e and q_t are the adsorption amounts of dyes at equilibrium contact time and t min, respectively.

3. Results and discussion

3.1. Characterization of expanded graphite and EG-64Gel microbeads

3.1.1. FT-IR spectra

In FT-IR spectra of natural graphite and expanded graphite (Fig. 1a), bands at 2,353; 669 cm^{-1} represented

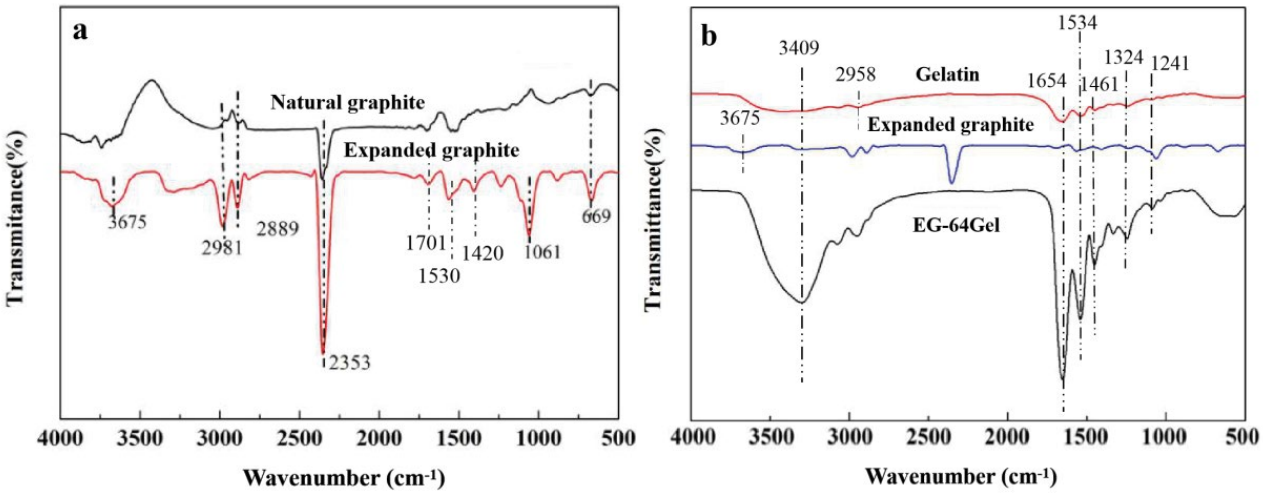

Fig. 1. FT-IR spectra of various adsorbents.

C-O–C and C–H stretching vibration, respectively. The –CH_2 stretching vibration could be observed at 2,981 and 2,889 cm^{-1} [23]. A broad band at around 3,675 cm^{-1} confirmed the existence of O–H group and adsorbed water, the peak centered at 1,701 cm^{-1} was ascribed to C=O group [24], bands at 1,530 and 1,420 cm^{-1} attributed to –COOH stretching vibration, indicating that those oxygen-containing functional groups formed during the oxidation of natural graphite. The absorption peak at 1,061 cm^{-1} attributed to the characteristic of SO_4^{2-}, indicating that sulfate or sulfuric acid intercalated into graphite layer [25,26].

FT-IR spectra of expanded graphite, gelatin and EG-64Gel are presented in Fig. 1b. For gelatin, a broad band at 3,409 cm^{-1} was assigned to the stretching vibration of N–H bond, bands at 2,958 and 1,461 cm^{-1} represented the stretching and bending vibrations of C–H, respectively; the characteristic peak at 1,654 cm^{-1} was attributed to the stretching vibration of the carbonyl group of amide I; and the medium peak at 1,534 cm^{-1} presented the bending vibration of N–H bond of amide II [27,28]. The weak bands at 1,324 and 1,241 cm^{-1} were assigned to C–N bond stretching vibration [29]. These characteristic bands were also observed in EG-64Gel, indicated that layered structure of EG was maintained. Further, the intensity of the peak attributed to the stretching vibration of N–H bond in gelatin at 3,409 cm^{-1} was enhanced significantly in EG-64Gel, indicating the interaction between EG and gelatin [30].

3.1.2. SEM images

A compact, stacked layer and scaly structure with orderly surface was observed for natural graphite (Fig. 2a), whereas expanded graphite exhibited a characteristic homogeneous dilation and vermicular structure with lots of V-type pores on the surface, with open or semi-open, interconnected pores, mostly in the shape of slit and wedges, and the pore size ranged from dozens of microns to hundreds of microns (Fig. 2b) [31]. Such special loosely bonded, porous vermicular structure of EG increased its surface and the pollutants could be adsorbed more easily and thus favorable for adsorption. A spherical smooth surface was observed for gelatin beads (Fig. 2c). The obtained EG-64Gel composite beads showed relatively uniform spherical with well dispersion and basically maintained the surface characteristic of gelatin (Fig. 2d), which may be due to the small amount of EG. The relatively uniform spherical beads should benefit to its separation from the liquid system.

3.1.3. TGA

TGA curves of various materials are presented in Fig. 3. Almost no mass loss was observed from room temperature to 800°C for natural graphite, indicating that natural graphite applied was in high purity in this research. Whereas expanded graphite underwent roughly several stages [32]: the first stage took place in the range of 60°C–200°C with about 18% mass loss attributing to the physical adsorbed water molecules, the second stage took place at 200°C–600°C with about 10% mass loss attributing to the dehydration of bound water and the decomposition of part of oxygen-containing functional groups [23], which indicated that the expansion of expanded graphite occurred at the initial temperature of 200°C. The third stage with obvious mass loss about 50% took place between 600°C and 800°C, which could be ascribed to the decomposition of H_2SO_4 intercalation species and the burn of carbon skeleton [28]. TGA inferred that at least 50% of oxygen-functional groups in weight were introduced in EG structure during the expansion of natural graphite.

For gelatin, the first stage with about 18% mass loss was observed at the temperature lower than 200°C, corresponding to the physically adsorbed water molecules; then at the range of 200°C–500°C gelatin underwent thermal cracking [28]. EG-64Gel composite beads exhibited the similar TG curve to gelatin, the second stage of mass loss with 48% corresponded to the thermal cracking of gelatin, and the third stage corresponded to the oxidation decomposition of carbon skeleton in EG, with mass loss of 34%. These results showed that the thermal stability of EG-64Gel composite beads was similar to that of gelatin, and demonstrated that

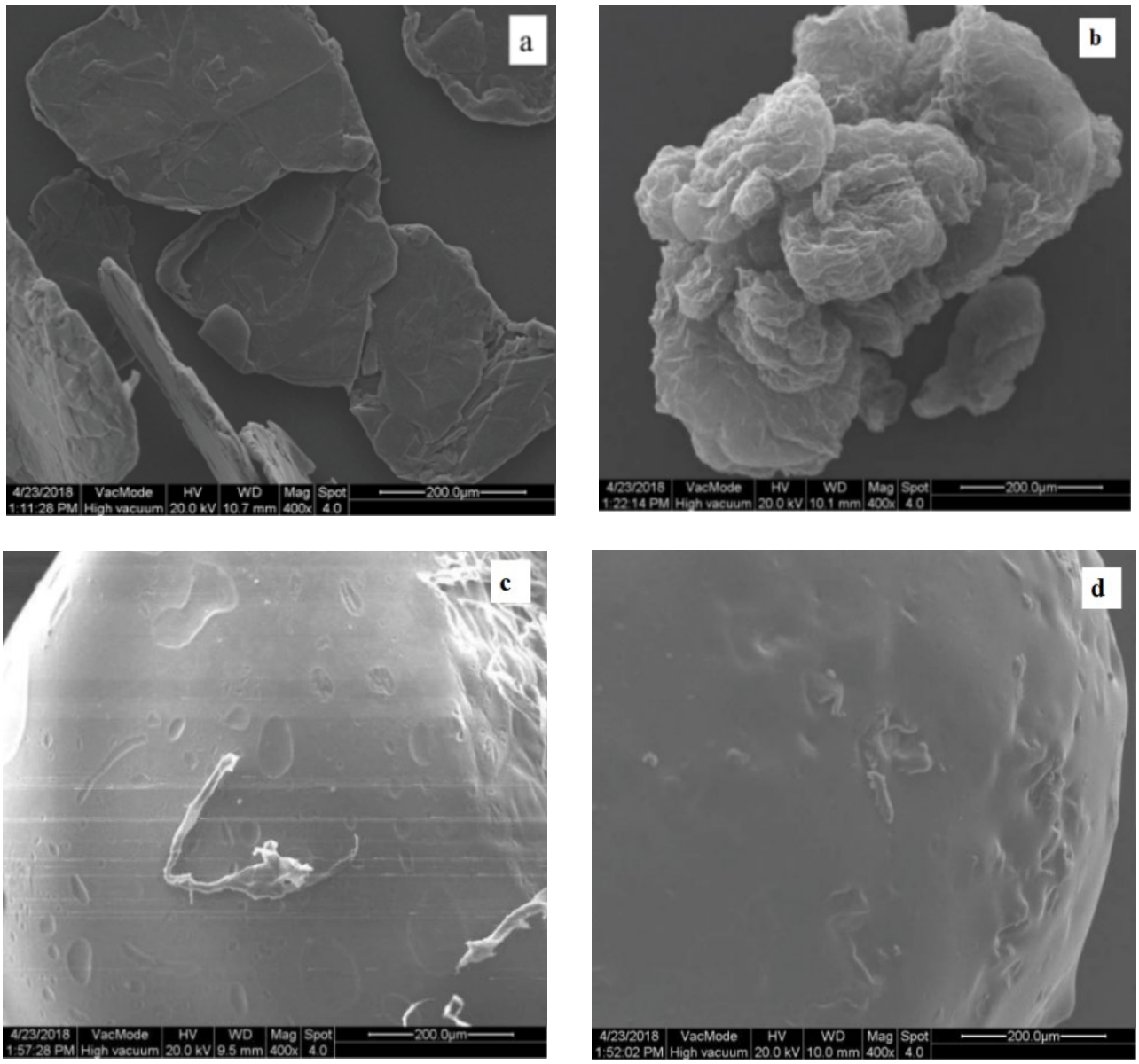

Fig. 2. SEM images of (a) natural graphite, (b) expanded graphite, (c) gelatin, and (d) EG-64Gel.

the composite beads adsorbent could be applied in a wide temperature range.

3.2. Optimizing preparation parameters for expanded graphite

Expanded graphite was derived from natural flake graphite by oxidizing and intercalating with $(NH_4)_2S_2O_8$/H_2SO_4 at room temperature, following by ultrasonic, drying for further expansion. By providing unique reaction conditions and generating bubbles via acoustic cavitation with effectively accumulating the diffuse energy, ultrasound has been widely used in the synthesis of nanostructured materials [33]. In general, the larger the expansion volume, the more the amount of worm vacuum and μm pore structure, and the higher adsorption capacity [34]. Here the influence of ultrasound time (t_U), drying temperature (T_D) and drying time (t_D) on the expansion volume of EG was studied (Fig. 4). As can be seen from Fig. 4a, the expansion volume of expanded graphite without ultrasound treatment during the preparation process was 110.0 mL. With the increase of ultrasound time, the expansion volume increased constantly and reached the maximum of 189.3 mL g^{-1} at 40 min, then decreased with further extending. This might be due to the generation of bubbles by acoustic cavitation with effectively accumulating the diffusion energy, the interlayer interaction of natural graphite was broken by the released energy derived from the transient, localized hot spots and began to expand, then the intercalation agent also entered the graphite interlayer, and natural graphite continued to expand [34]. So the oxidation process and expansion were enhanced by the extreme micro-environment of high temperature and pressure from the cavitation and mechanical effects of

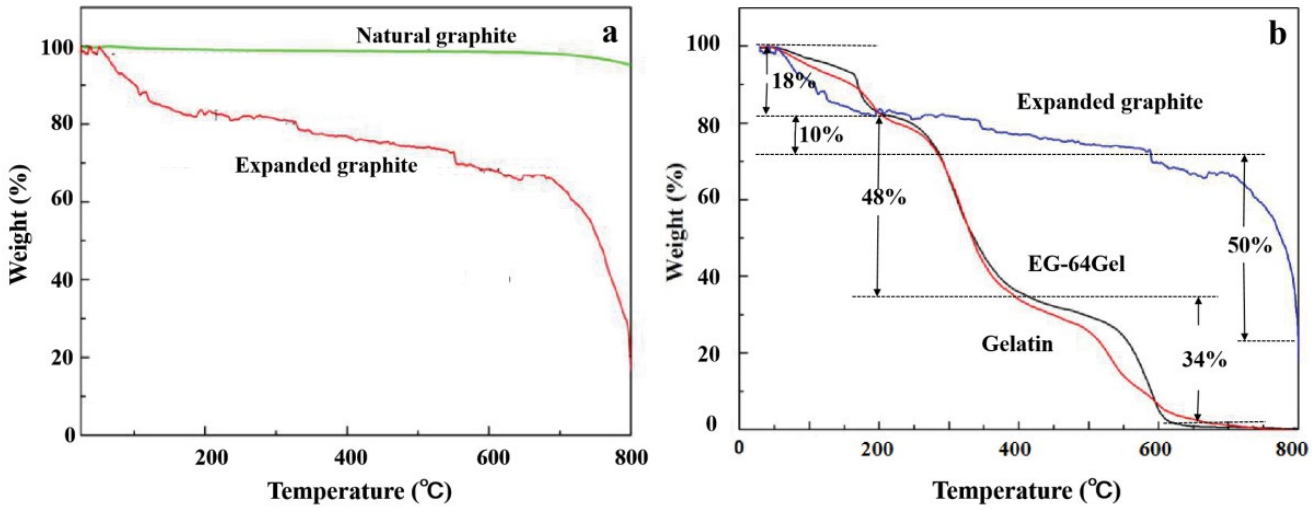

Fig. 3. TGA curves of natural graphite, expanded graphite, gelatin and EG-64Gel.

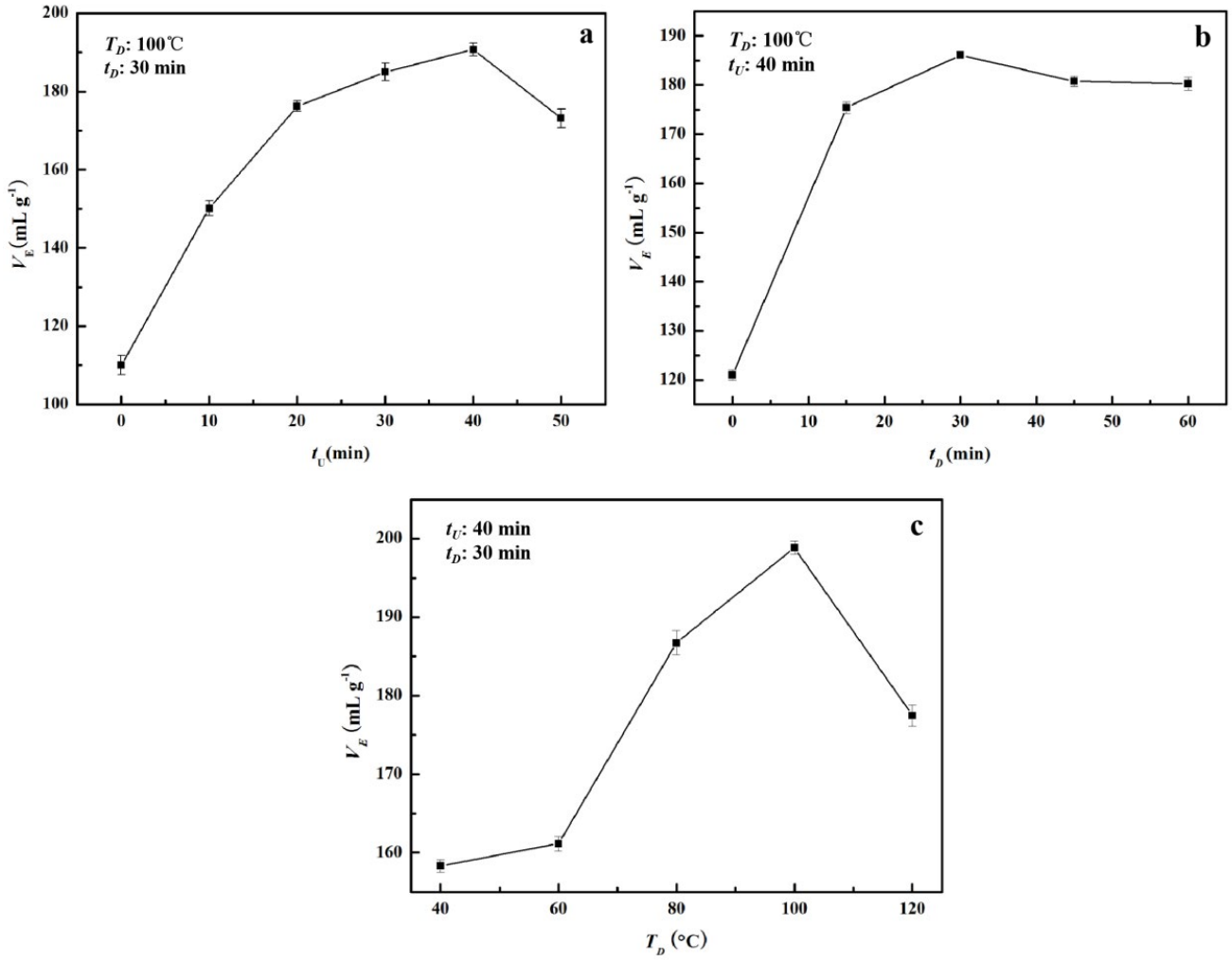

Fig. 4. Effects of (a) ultrasonic time, (b) drying time, and (c) temperature on the expansion volume of expanded graphite.

ultrasound [35]. However, the particles will re-aggregate with long time treatment, which results in insufficient reaction of the mixed solution and slightly reduced expansion volume [36].

After treated by ultrasonic for 40 min, EG volume expanded up to 120 mL g^{-1}, then dried the sample at 100°C and recorded the expansion volume at every 15 min, the results are shown in Fig. 4b. The expansion volume increased gradually and reached 185.2 mL g^{-1} at 30 min, and then basically kept stable, suggesting that the intercalation and expansion process further proceeded with time increasing, even if ultrasound stopped.

When the drying temperature increased from 40°C to 100°C, the expansion volume increased from 157.5 to 199.7 mL g^{-1}, and then decreased with the temperature further rising (Fig. 4c). This might be because that with the increase of temperature, the molecular motion was accelerated, thus the expansion volume increased. When the temperature was too high, the inserted species tend to run out from the layer of EG, so the expansion volume reduced [37,38].

To sum up, mild oxidation and intercalation of natural graphite with $(NH_4)_2S_2O_8/H_2SO_4$ at room temperature followed by ultrasonic for 40 min and dried at 100°C for 30 min, the largest expansion volume of 199.7 mL g^{-1} of EG was obtained.

3.3. Evaluation of adsorption performance of expanded graphite

3.3.1. In single-oil system

Under the same conditions, the adsorption performance of EG toward five different oily substrates was studied at room temperature (Fig. 5a). The adsorption quantity of EG was different and reached 23.89, 26.03, 21.01, 14.54 and 18.59 g g^{-1}, for engine oil, edible oil, benzene, *n*-heptane and *p*-xylene, respectively, within 30 min. The highest adsorption quantity toward edible oil was obtained, indicating that the adsorption capacity of EG was closely related with the type of the substrates. In terms of composition, benzene, *p*-xylene and *n*-heptane are pure substances, both benzene and *p*-xylene have π bonds in their structure, which are conducive to interact with EG by π–π interaction. Therefore, the adsorption capacities of EG toward benzene and *p*-xylene were superior to that of *n*-heptane. However, the main

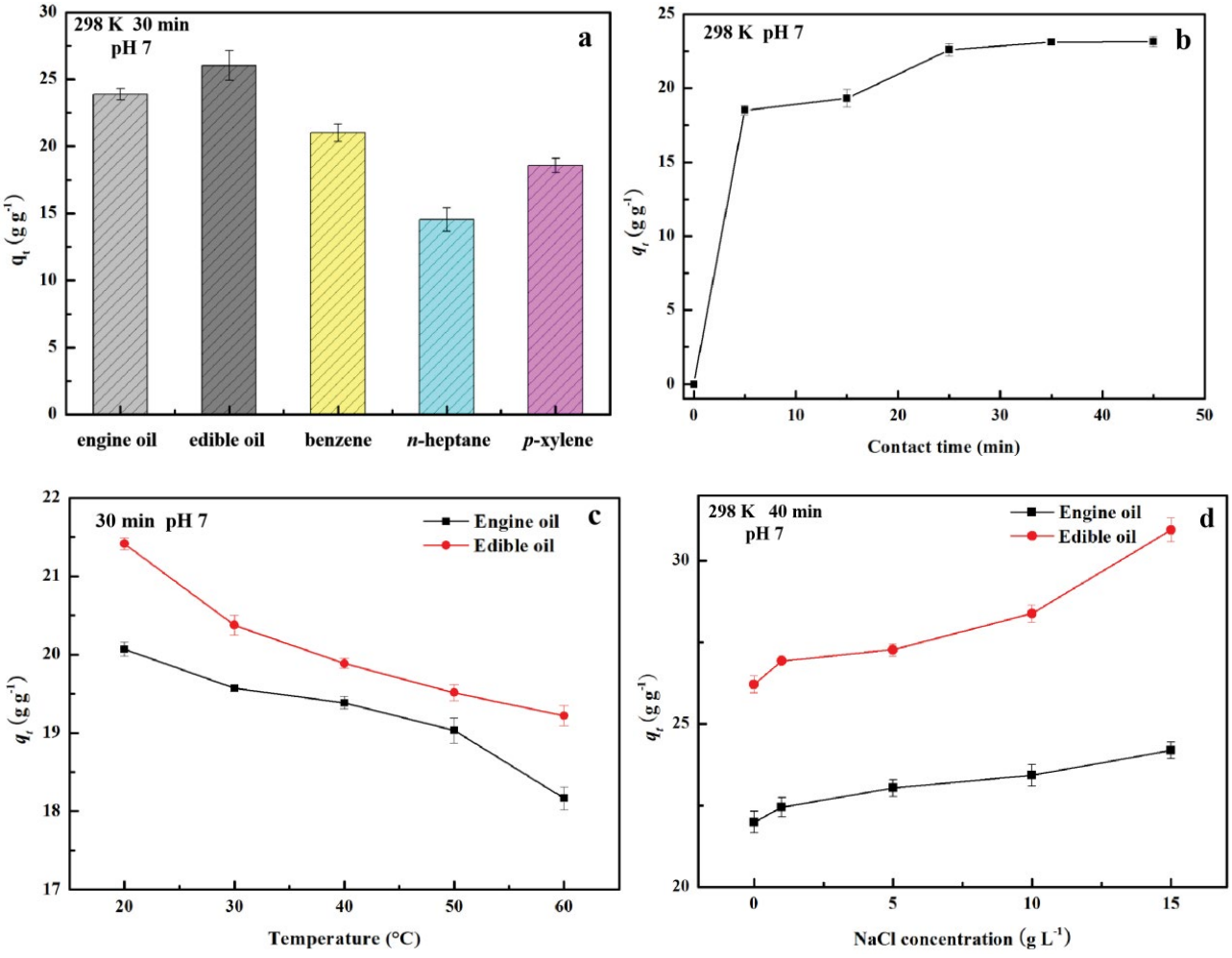

Fig. 5. Adsorption properties of expanded graphite for oily substrates in a single oil (a) and oily wastewater system ((b) contact time; (c) temperature; and (d) NaCl concentration).

components of edible oil and engine oil are unsaturated fatty acids, triglycerides, hydrocarbon substances, etc., the higher adsorption capacities might due to the comprehensive interaction of π–π and electronic attraction between the oxygen-containing functional groups. In addition, the viscosity of edible oil (180 mpa s) was higher than that of engine oil (156 mpa s), indicating that the adsorption amount of EG increased with the viscosity of the oily substrates increase. Comparing the adsorption amount with reported [32,40,41] sulfuric intercalated EG adsorbents toward oily substrates (Table 1), the EG prepared in this study acted as an excellent adsorbent with moderate adsorption performance for oil-based substances. This might be due to the destruction of its characteristic worm-like structure during the adsorption. These results demonstrated that the prepared EG exhibited excellent adsorption capacities toward the substrates with more π bond and higher viscosity.

3.3.2. In oily wastewater system

In the edible oil–water binary system, the adsorption quantity increased with the contact time increasing and reached 23.05 g g^{-1} within 30 min, and then gradually kept stable (Fig. 5b). This was mainly because the adsorption site basically reached saturation, so the contact time in subsequent experiments was 30 min.

With the temperature rising, EG adsorption amount in edible oil–water and engine oil–water systems decreased gradually from 21.64 and 20.18 g g^{-1} at 20°C to 19.44 and 18.21 g g^{-1}, respectively, at 60°C (Fig. 5c). This result indicated that the adsorption process was exothermic [40], lower temperature was conducive to the adsorption of the oily substrates. This phenomenon might be related with the decrease in viscosity and increase in fluidity of oil with temperature increasing, which was unfavorable to the adhesion of oil to EG [39]. The higher adsorption capacity of EG to edible oil might also be attributed to the higher viscosity of edible oil. Considering the difference was insignificant, EG should be used in a wide range of temperature.

Table 1
Comparison of oily substrates onto sulfuric intercalated expanded graphite

Oily substrates	Adsorption amount q_t (g g^{-1})				Viscosity (mpa·s)
Diesel oil	5.15	37.26	50.879		8
Crude oil	5.54	40.46	65.537		626
Engine oil	6.32	41.46	55.128	23.89	156
Gasoline	4.00	31.96	43.25		1
Kerosene			47.657		2
Gear oil			84.681		1,407
Edible oil				26.03	180
Benzene				21.01	0.652
n-Heptane				14.54	0.4
p-Xylene				18.59	0.648
Reference	[40]	[41]	[32]	This study	

The influence of NaCl concentration showed that the adsorption quantity of EG increased from 22.25 to 23.97 g g^{-1}, and 26.38 to 30.92 g g^{-1} toward engine and edible oil, respectively, with increase of NaCl concentration from 0 to 15 g L^{-1} (Fig. 5d). Moreover, the enhancement of edible oil was higher than that of engine oil. On one hand, it might be due to that the higher ionic strength reduced the solubility of the adsorbate in the solution, which was more conducive to the migration of the adsorbate from the liquid phase to the solid phase surface [41]. On the other hand, the interaction between the introduced NaCl and edible oil with more oxygen-containing polar component was stronger than that of engine oil with more nonpolar constitutes, thus increased the viscosity and improved the adsorption capacity. Therefore, the adsorption efficiency of EG in oil–water binary system with higher salinity was higher than that of lower salinity, which were consistent with literature reports [42]. These results indicated that EG was suitable for oil leakage accidents treatment under high salinity conditions, especially for the treatment of marine petroleum pollution.

3.4. Evaluation on adsorption performance of EG-xGel

3.4.1. Effects of various parameters on methylene blue and Congo red removal

To remove various dyes in wastewater with EG-based adsorbent, EG-*x*Gel composite microbeads with various EG to gelatin ratio, labeled as EG-64Gel, EG-48Gel and EG-24Gel, were synthesized and the comparison of adsorption performance was shown in Fig. 6a. Under the same conditions, the removal efficiency of methylene blue (MB) and congo red (CR) by the single gelatin was 61.3% and 47.4%, respectively; whereas for EG, 40.2% and 80.7% removal were observed for MB and CR, respectively. These results indicated that the single-component adsorbent exhibited good adsorption capacities toward dye molecules. Moreover, it was found that higher anionic CR removal by EG with positive charged surface and cationic MB removal by gelatin with negative charged surface, further suggesting that the electrostatic attraction plays an important role during the adsorption process [43]. However, with the composite microbeads as adsorbent, especially EG-64Gel, 68.2% MB and 79.2% CR removal could be obtained, superior to that of single gelatin and EG, indicating that excellent adsorption capacity of the single component was integrated into the composite beads adsorbent. Moreover, the granulating effect of microbeads was beneficial to separate from the liquid–solid system and recycle in the real industry application. Therefore, EG-64Gel microbeads were further investigated.

The influence of contact time (Fig. 6b) showed that MB removal gradually increased with the increase of contact time within 120 min, and then reached the adsorption equilibrium. For CR dye, the removal increased rapidly in the initial 40 min, then followed by a slight decrease. This was because at the initial stage of adsorption, there were a large number of vacant active adsorption sites on the surface of the microbeads available for the dye molecules. With the extension of contact time, the active adsorption sites were gradually occupied and reduced, and the adsorption process reached

equilibrium. Second, as the adsorption mainly occurred on the surface of composite microbeads, when the adsorbed dye reached a certain amount, the steric effect might also lead to a relatively gentle decline of the dye removal [44]. Therefore, the optimal contact time for MB and CR at 120 and 40 min with the maximum removal of 68.2% for MB and 87.2% for CR was obtained, respectively.

At acidic conditions (pH = 3), higher anionic CR and lower cationic MB removal were observed (Fig. 6c), due to that a large number of H^+ resulted in the surface of the protonated microbeads positively charged, which was consistent with zeta potential analysis. With the solution pH increasing, zeta potential of EG-64Gel gradually decreased from +30.7 mV at pH 3 to –38.5 mV at neutral condition,

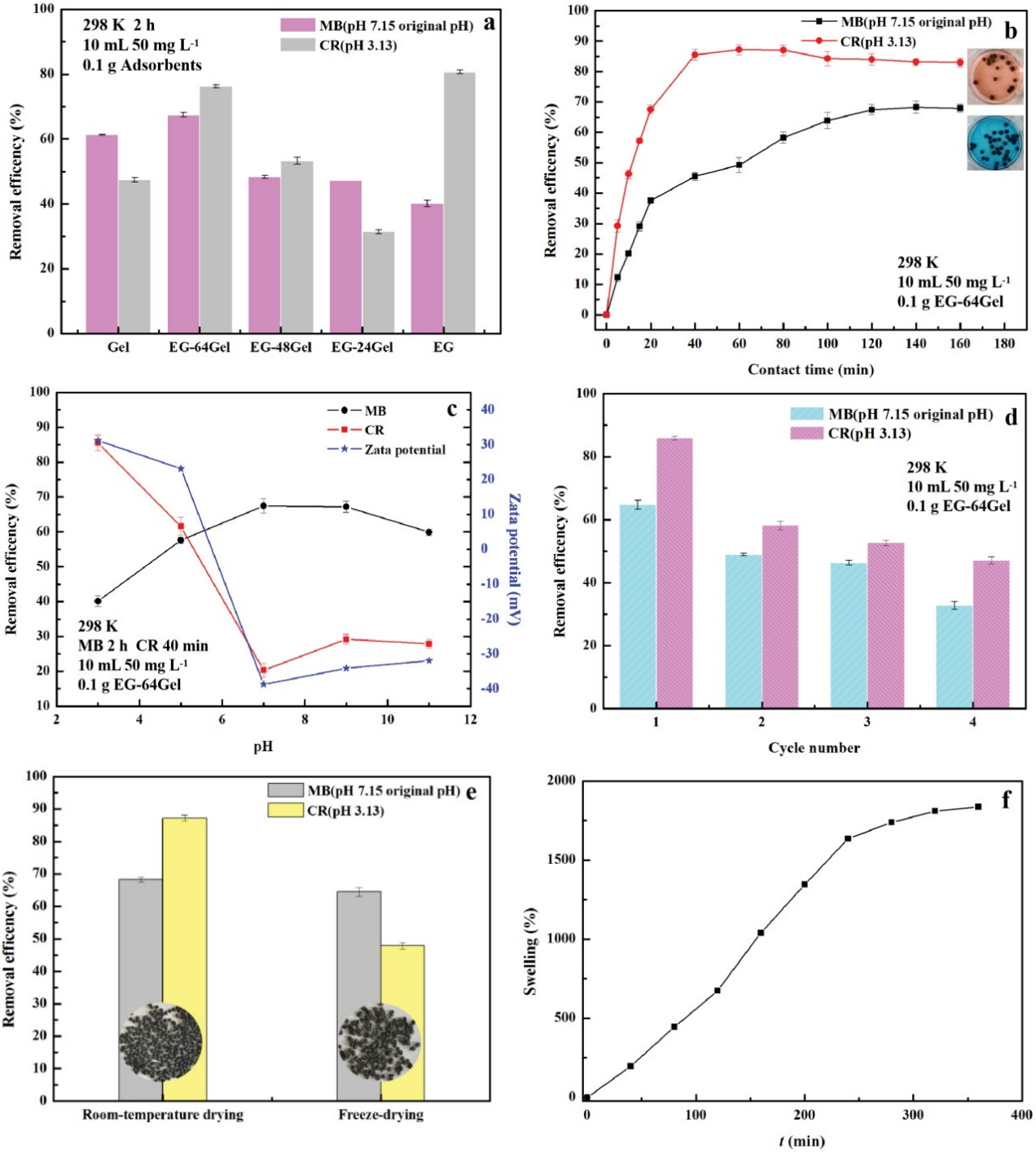

Fig. 6. Effects of various parameters on methylene blue and congo red removal ((a) component; (b) contact time; (c) pH; (d) recycle of EG-64Gel; (e) drying way; and (f) swelling of EG-64Gel).

and then increased to –32.7 mV at pH 11. This might attribute to the amine group protonated (–NH_2 exists as –NH_3^+) at the acidic condition, resulting in the surface of the adsorbent positively charged and the pH of zero point of charge (pH_{zpc}) was about 6 [45]. Therefore, the enhancement of electrostatic interaction with anionic dye CR was conducive to its adsorption, while the electrostatic repulsion hindered the adsorption of cationic MB. With the increase of pH value, opposite results were obtained due to the ionization of –COOH and the composite was negatively charged [46]. On the other hand, gelatin is an amphoteric natural polymer, so EG-64Gel composite microbeads also exhibited amphoterism at different pHs.

The recycle of EG-64Gel microbeads (Fig. 6d) showed that after recycling for four times, MB and CR removal decreased obviously from 64.1% and 85.9% to 33.5% and 47.2%, respectively. This might be due to that the occupied adsorption sites of the composite microbeads were not completely desorbed, which was not conducive to the recycle of the adsorbent, and effective desorption method need to be explored.

EG-64Gel composite microbeads were dried and the effect of the drying way is shown in Fig. 6e. Uniform size and compact structure with good integrity and dispersion were observed for air drying at room temperature, while irregular larger size microbeads with 1.5 mm in diameter were observed for freeze drying. No obvious differences in MB removal were observed; however, a distinct higher CR removal was observed for air drying at room temperature, which might be due to the larger diameters and lower specific surface area of the freeze-drying sample [47].

The swelling of EG-64Gel in water in Fig. 6f shows that at the initial stage, the swelling increased and then almost unchanged after 300 min. This was due to the three-dimensional spiral structure of gelatin linked by hydrogen bonding, which was weakened by the insertion of water molecules, then led to swelling and finally reached equilibrium. The results showed the strong water absorption capacity of EG-64Gel microbeads, which was conducive to the adsorption of dye molecules [48].

Although a comparable adsorption performance of EG-64Gel was obtained when compared with references reported [49–53], due to its tunable adsorption capacity, low cost and fast separation efficiency, EG-64Gel microbeads should act as an alternative adsorbent material in the future.

3.4.2. Selective adsorption properties of EG-64Gel in MB/CR binary system

The UV-vis spectra of MB/CR binary system at various pHs and NaCl concentrations are shown in Fig. 7. At the original pH (pH 7.23), the absorbance of CR was almost unchanged, while that of MB decreased with time increased from 10 to 120 min (Fig. 7a), suggesting that the composite microbeads exhibited selective adsorption capacity toward MB. While at acidic condition (pH 3.13, Fig. 7b),

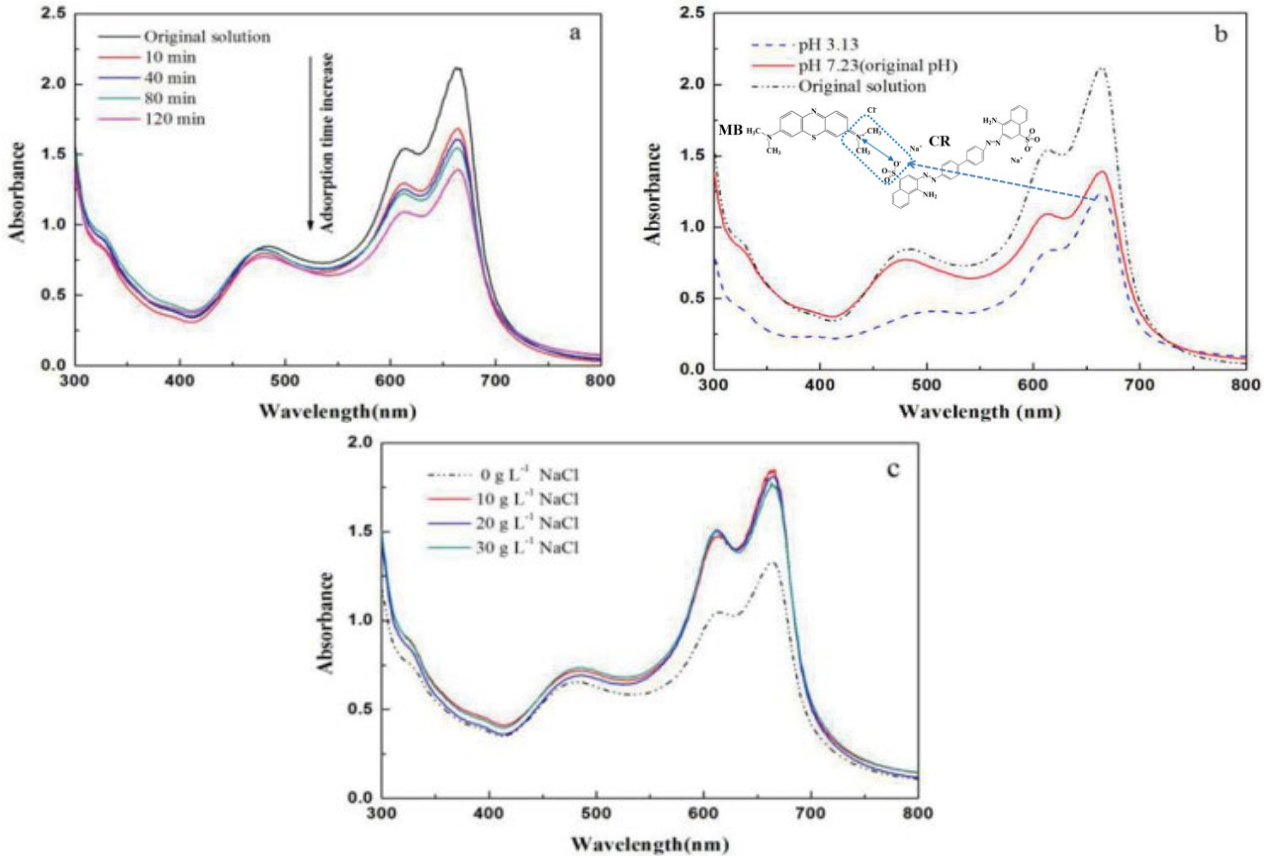

Fig. 7. Effects of (a) contact time, (b) pH, and (c) NaCl on MB/CR adsorption (0.10 g EG-64Gel; 10 mL 50 mg L^{-1} dye; room temperature).

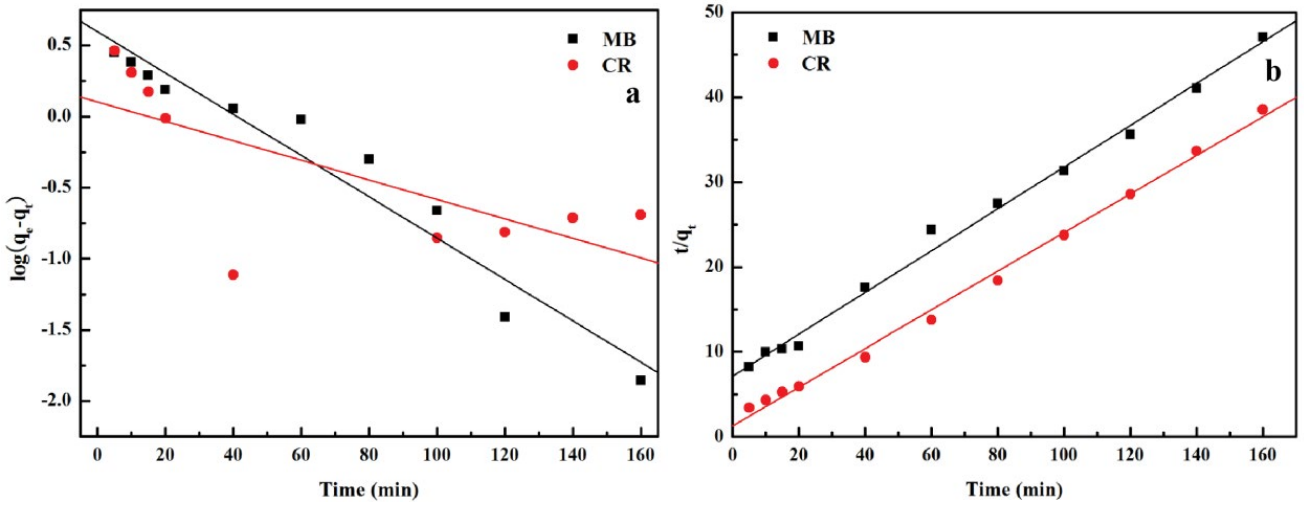

Fig. 8. Pseudo-first-order (a) and pseudo-second-order and (b) kinetics plot for methylene blue and congo red adsorption onto EG-64Gel.

Table 2
Kinetic parameters for MB and CR adsorption onto EG-64Gel

Dyes	$q_{e,max}$ (mg g^{-1})	Pseudo-first-order model			Pseudo-second-order model		
		$q_{e,1}$ (mg g^{-1})	k_1 (min^{-1})	R^2	$q_{e,2}$ (mg g^{-1})	k_2 (g m-g^{-1} min^{-1})	R^2
MB	3.412	3.950	0.0334	0.9482	4.064	0.0605	0.9940
CR	4.359	1.268	0.0158	0.5172	4.399	0.0517	0.9958

CR was almost removed completely, and MB removal was also higher than original neutral pH at the individual system (Fig. 6c). It may be due to that the anionic sulfonate group in CR might interact with the co-existed cationic dye of MB, inferred that the co-existed cationic dye with opposite charges exhibited a marginal effect on the adsorption of anionic dye onto EG-64Gel under acidic condition, while the co-existed anionic dye exhibited a promoting effect on the adsorption of cationic dye. This result might be explained by the electrostatic attraction between the preferential adsorbed CR and MB molecules, and the positive charged surface of the EG-64Gel composite beads [44]. So excellent separation performance of EG-64Gel was exhibited under acidic condition, thus the selective adsorption property of composite microbeads in binary system could be achieved facilely by adjusting the initial pH of solution.

The adsorption performances of composites toward two dyes both were inhibited thoroughly in the presence of NaCl as Fig. 7c shown, perhaps because with the increase of ionic strength, more charged active sites on the adsorbent were shielded by Na^+ and Cl^- ions, thus led to the enhanced electrostatic repulsion interaction between adsorbent and adsorbate, and deteriorated the adsorption performance of composite microbeads [50].

3.5. Adsorption kinetics

Adsorption kinetics was used to analyze the adsorption rate of MB and CR onto EG-64Gel composite and the possible adsorption mechanism. The kinetic plots and parameters are given in Fig. 8 and Table 2, respectively. The experimental data fitted better with the pseudo-second-order than the pseudo-first-order model, with higher linear coefficient (R^2) and the calculated adsorption quantity ($q_{e,2}$) was closer to the experimental value ($q_{e,exp}$). These results showed that chemisorption was the rate-limiting step and involved in the adsorption process [22].

4. Conclusion

New eco-friendly adsorbent EG and EG-*x*Gel with high adsorption efficiency was prepared successfully and used for oily substrates and dyes removal from water, respectively. The adsorption quantities of EG toward engine oil, edible oil, benzene, *n*-heptane and *p*-xylene were 23.89, 26.03, 21.01, 14.54 and 18.59 g g^{-1}, respectively, indicated that EG exhibited excellent adsorption capacities toward the oily substrates with more π bond and higher viscosity. In oily wastewater system, the maximum adsorption quantities of EG toward engine and edible oil were 23.97 and 30.92 g g^{-1}, respectively, in the presence of 15 g L^{-1} NaCl at 20°C within 30 min; this demonstrated that EG could act as a potential adsorbent in marine oil pollution treatment. By comparing the adsorption performance of composite microbeads EG-*x*Gel toward MB and CR, the ratio of EG to gelatin at 1:64 was optimized. FT-IR showed that EG and gelatin were successfully combined by physical interaction. SEM images showed that a regular shape, smooth surface and good dispersion were observed for EG-64Gel microbeads. The possible adsorption mechanism could be explained mainly by electrostatic

attraction and the kinetics results showed that chemisorption was the rate-limiting step and involved in the adsorption process. Better separation performance of EG-64Gel was observed under acidic condition in MB/CR binary system. The addition of NaCl inhibited the adsorption of MB and CR, perhaps because the charged active sites of adsorbent were shielded by the increase of ionic strength. All these results demonstrated that EG-*x*Gel microbeads could act as a potential effective adsorbent in oil leaking accidents and industrial dyes wastewater treatment.

References

[1] C. Drevon, Marine oils and their effects, Nut. Rev., 50 (1992) 38–45.

[2] J. Jackson, J. Cubit, B. Keller, V. Batista, K. Burns, H. Caffey, R. Caldwell, S. Garrity, C. Getter, C. Gonzalez, Ecological effects of a major oil spill on panamanian coastal marine communities, Science, 243 (1989) 37–44.

[3] A. Jernelov, How to defend against future oil spills, Nature, 466 (2010) 182–183.

[4] C. Peterson, S. Rice, J. Short, D. Esler, J. Bodkin, B. Ballachey, D. Irons, Long-term ecosystem response to Exxon Valdez oil spill, Science, 302 (2003) 2082–2086.

[5] L. Yuan, L. Han, W. Bo, H. Chen, W. Gao, B. Chen, Simulated oil release from oil-contaminated marine sediment in the Bohai Sea, China, Mar. Pollut. Bull., 118 (2017) 79–84.

[6] L. Jing, X. Gong, D. Qiao, B. Wang, D.F. Han, X. Zhang, Review of the impact of oil pollution on the food security of marine shellfish, Fis. Qual. Stand., 1 (2015) 47–53.

[7] M. Lin, Marine environmental protection: a highly efficient method of degradation of heavy oil pollution on coastal beaches, Hydrol. Curr. Res., 7 (2016) 231–233.

[8] M. Hubbe, O. Rojas, M. Fingas, B. Gupta, Cellulosic substrates for removal of pollutants from aqueous systems: a review, Bioresources, 7 (2012) 2592–2687.

[9] S.N. Jain, P.R. Gogate, Adsorptive removal of azo dye in a continuous column operation using biosorbent based on NaOH and surfactant activation of *Prunus dulcis* leaves, Desal. Wat. Treat., 141 (2019) 331–341.

[10] S.N. Jain, P.R. Gogate, Efficient removal of Acid Green 25 dye from wastewater using activated *Prunus dulcis* as biosorbent: batch and column studies, J. Environ. Manage., 210 (2018) 226–238.

[11] R. Sarbatly, D. Krishnaiah, Z. Kamin, A review of polymer nanofibres by electrospinning and their application in oil-water separation for cleaning up marine oil spills, Mar. Pollut. Bull., 106 (2016) 1–8.

[12] S.N. Jain, P.R. Gogate, Adsorptive removal of acid violet 17 dye from wastewater using biosorbent obtained from NaOH and H_2SO_4 activation of fallen leaves of Ficus racemosa, J. Mol. Liq., 243 (2017) 132–143.

[13] Y. Sun, C. Ding, W. Cheng, X. Wang, Simultaneous adsorption and reduction of U(VI) on reduced graphene oxide-supported nanoscale zerovalent iron, J. Hazard. Mater., 280 (2014) 399–408.

[14] C. Ding, W. Cheng, Y. Sun, X. Wang, Novel fungus-Fe_3O_4 bio-nanocomposites as high performance adsorbents for the removal of radionuclides, J. Hazard. Mater., 295 (2015) 127–137.

[15] Z. Chen, C. Liu, Y. Zhang, T. Qiu, X. Liu, Dynamic adsorption of expanded graphite for oil in waste water of oil field, Mater. Mech. Eng., 30 (2006) 81–83.

[16] S.J. Park, S.Y. Lee, K.S. Kim, F.L. Jin, A novel drying process for oil adsorption of expanded graphite, Carbon Lett., 14 (2013) 193–195.

[17] J. Li, M. Li, J. Li, Removal of disperse blue 2BLN from aqueous solution by combination of ultrasound and exfoliated graphite, Ultrason. Sonochem., 14 (2007) 62–66.

[18] Y. Wan, Y. Wang, K. Yao, Carbon fiber-reinforced gelatin composites. II. Swelling behavior, J. Appl. Polym. Sci., 75 (2015) 994–998.

[19] T. Liu, R. Zhang, X. Zhang, K. Liu, Y. Liu, One-step room-temperature preparation of expanded graphite, Carbon, 119 (2017) 544–547.

[20] T. Peng, B. Liu, X. Gao, Preparation, quantitative surface analysis, intercalation characteristics and industrial implications of low temperature expandable graphite, Appl. Surf. Sci., 444 (2018) 800–810.

[21] R. Koswojo, R. Utomo, Y. Ju, A. Ayucitra, F. Soetaredjo, J. Sunarso, S. Ismadji, Acid Green 25 removal from wastewater by organo-bentonite from Pacitan, J. Appl. Clay Sci., 48 (2010) 81–86.

[22] W. Weber, J. Morris., Kinetics of adsorption on carbon from solution, J. Sanit. Eng. Div. Am. Soc. Civ. Eng., 1 (1963) 1–2.

[23] Y. Ma, Y. Ruan, D. Xing, X. Du, P. La, Fabrication of amino functionalized magnetic expanded graphite nanohybrids for application in removal of Ag(I) from aqueous solution, J. Nanomater., 2017 (2017) 1–11.

[24] C. Xu, Y. Jiao, S. Hou, H. Jin, L. Min, Z. Ji, Research on removal of fluoride in aqueous solution by alumina-modified expanded graphite composite, J. Alloy. Compd., 620 (2015) 361–367.

[25] C. Xu, W. Yang, W. Liu, Performance and mechanism of Cr(VI) removal by zero-valent iron loaded onto expanded graphite, J. Environ. Sci., 67 (2018) 14–22.

[26] W. Jiang, J. Fang, Z. Li, X. Yang, L. Lu, P. Cha, Preparation and study of spectra characteristics of expandable graphite, J. Funct. Mater., 41 (2010) 200–203.

[27] E. Duhoranimana, E. Karangwa, L. Lai, X. Xu, J. Yu, S. Xia, X. Zhang, B. Muhoza, I. Habinshuti, Effect of sodium carboxymethyl cellulose on complex coacervates formation with gelatin: coacervates characterization, stabilization and formation mechanism, Food Hydrocoll., 69 (2017) 111–120.

[28] M. Khannam, R. Boruah, S. Dolui, An efficient quasi-solid state dye sensitized solar cells based on graphene oxide/gelatin gel electrolyte with NiO supported TiO_2 photoanode, J. Photochem. Photobiol., 335 (2017) 248–258.

[29] C. Zhuang, F. Tao, Y. Cui, Anti-degradation gelatin films crosslinked by active ester based on cellulose, RSC Adv., 5 (2015) 52183–52193.

[30] S. Saber-Samandari, H. Joneidi-Yekta, M. Mohseni, Adsorption of anionic and cationic dyes from aqueous solution using gelatin-based magnetic nanocomposite beads comprising carboxylic acid functionalized carbon nanotube, Chem. Eng. J., 308 (2017) 1133–1144.

[31] W. Cui, J. Chen, C. Xie, Feasibility study on preparation of graphene by exfoliated graphite, Front Sci. Ser., 5 (2011) 40–47.

[32] L. Wang, X. Fu, E. Chang, H. Wu, K. Zhang, X. Lei, R. Zhang, X. Qi, Y. Yang, Preparation and its adsorptive property of modified expanded graphite nanomaterials, J. Chem., 2014 (2014) 1–5.

[33] P. Gogate, Cavitational reactors for process intensification of chemical processing applications: a critical review, Chem. Eng. Process., 47 (2008) 515–527.

[34] J. Li, M. Li, Preparation of expandable graphite with ultrasound irradiation, Mater. Lett., 61 (2007) 5070–5073.

[35] H. Jin, K. Suslick, Applications of ultrasound to the synthesis of nanostructured materials, Adv. Mater., 22 (2010) 1039–1059.

[36] J. Li, C. Mi, J. Li, Y. Xu, Z. Jia, M. Li, The removal of MO molecules from aqueous solution by the combination of ultrasound/adsorption/photocatalysis, Ultrason. Sonochem., 15 (2008) 949–954.

[37] W. Fu, Preparation and oil adsorption capacity of sulfur-free expanded graphite, Chin. J. Environ. Eng., 6 (2012) 1518–1524.

[38] F. An, L. Luo, B. Liu, Preparation and characterization of sulfur-free expansible graphite, J. Mod. Chem. Ind., 37 (2017) 75–79.

[39] C. Xu, C. Jiao, R. Yao, A. Lin, W. Jiao, Adsorption and regeneration of expanded graphite modified by CTAB-KBr/H_3PO_4 for marine oil pollution, Environ. Pollut., 233 (2018) 194–200.

[40] G. Wang, Q. Sun, Y. Zhang, Sorption and regeneration of magnetic exfoliated graphite as a new sorbent for oil pollution, Desalination, 263 (2010) 183–188.

[41] Y. Hao, H. Teng, X. Gu, Application of expanded graphite to the treatment of low concentrated oil-bearing wastewater, Ind. Water. Treat., 30 (2010) 714–719.

[42] Y. Hu, T. Guo, X. Ye, Q. Li, G. Quan, H. Liu, Dye adsorption by resins: effect of ionic strength on hydrophobic and electrostatic interactions, Chem. Eng. J., 228 (2013) 392–397.
[43] Q. Lin, M. Gao, J. Chang, Adsorption properties of crosslinking carboxymethyl cellulose grafting dimethyldiallylammonium chloride for cationic and anionic dyes, Carbohydr. Polym., 151 (2016) 283–294.
[44] E. Sara, N. Mehrdad, M.H.H. Seyed, Physical and mechanical properties of gelatin-CMC composite films under the influence of electrostatic interactions, Int. J. Biol. Macromol., 114 (2018) 1–9.
[45] L. Zeng, M. Xie, Q. Zhang, Chitosan/organic rectorite composite for the magnetic uptake of methylene blue and methyl orange, Carbohydr. Polym., 123 (2015) 89–98.
[46] S. Wu, Z. Bai, J. Xi, Preparation of gelatin microspheres by emulsification and heat cross-linking, J. Wuhan. Univ., 55 (2009) 555–558.
[47] C. Dong, S. Wei, Z. Duan, Swelling kinetics and cross-linking stability of gelatins with different gel strength, J. Chin. Pharm. Univ., 41 (2010) 435–440.
[48] L. Wang, J. Zhang, R. Zhao, Adsorption of basic dyes on activated carbon prepared from *Polygonum orientale* Linn: equilibrium, kinetic and thermodynamic studies, Desalination, 254 (2010) 68–74.
[49] W. Zou, S. Gao, L. Ke, Characterization of modified sawdust, kinetic and equilibrium study about methylene blue adsorption in batch mode, Korean. J. Chem. Eng., 30 (2013) 111–122.
[50] R. Ianos, C. Pacurariu, S.G.Muntean, E. Muntean, M.A. Nistor, D. Niznansky, Combustion synthesis of iron oxide/carbon nanocomposites, efficient adsorbents for anionic and cationic dyes removal from wastewaters, J. Alloys Compd., 741 (2018) 1235–1246.
[51] A. Karamipour, N. Rasouli, M. Movahedi, H. Salavati, A kinetic study on adsorption of Congo Red from aqueous solution by $ZnOZnFe_2O_4$-polypyrrole magnetic nanocomposite, Phys. Chem. Res., 4 (2016) 291–301.
[52] S. Dawood, T.K. Sen, Removal of anionic dye Congo red from aqueous solution by raw pine and acid-treated pine cone powder as adsorbent: equilibrium, thermodynamic, kinetics, mechanism and process design, Water Res., 46 (2012) 1933–1946.
[53] P.S. Kumar, S. Ramalingam, C. Senthamarai, M. Niranjanaa, P. Vijayalakshmi, S. Sivanesan, Adsorption of dye from aqueous solution by cashew nut shell: studies on equilibrium isotherm, kinetics and thermodynamics of interactions, Desalination, 261 (2010) 52–60.